Harnessing Photoenzymatic Reactions for Unnatural Biosynthesis in Microorganisms

Yujie Yuan[1,2,3†], Maolin Li[1,2,3†,#], Wesley Harrison[1,2,3], Zhengyi Zhang[1,2,3], Huimin Zhao[1,2,3,4,5*]

[1]DOE Center for Advanced Bioenergy and Bioproducts Innovation, University of Illinois Urbana-Champaign; Urbana, IL 61801, USA. [2]Department of Chemical and Biomolecular Engineering, University of Illinois Urbana-Champaign; Urbana, IL 61801, USA. [3]Carl Woese Institute for Genomic Biology, University of Illinois Urbana-Champaign; Urbana, IL 61801, USA. [4]NSF Molecular Maker Lab Institute, University of Illinois Urbana-Champaign; Urbana, IL 61801, USA. [5]NSF iBioFoundry, University of Illinois Urbana-Champaign; Urbana, IL 61801, USA.

[†]These authors contributed equally to this work.

[#]Present address: Frontier Science Center for the Creation of New Organic Substances, Nankai University, Tianjin, 300350, China

[*]Correspondence to: zhao5@illinois.edu

Abstract: Photobiocatalysis provides a powerful strategy for integrating light and biological catalysts to drive abiological transformations. However, its scalability is hindered by high enzyme loading, reliance on costly cofactors, and instability under radical-generating conditions. Here we report the integration of light-driven enzymatic reactions into the cellular metabolism of *Escherichia coli*, bridging flavin-based photobiocatalysis with biosynthesis. Using synthetic biology strategies, we engineered microbial cells to continuously produce olefin substrates and ene-reductase while regenerating cofactors directly from glucose. By externally supplying radical precursors or by introducing synthetic pathways for their *in situ* production, we enabled fermentation-based microbial photobiosynthesis, achieving high titres and demonstrating its feasibility for scale-up in bioreactor. This approach extends photobiocatalysis from *in vitro* applications to *in vivo* semi and complete biosynthesis, revealing its full potential for integrating light-driven reactions into cellular metabolism.

Main Text: Biosynthesis enables the precise assembly of complex molecules but remains limited by nature's enzymatic repertoire. Integrating new-to-nature reactivity into living systems offers a powerful means to expand chemical space and enable the rational design of non-natural products[1-9]. Photoenzymatic catalysis, which couples enzymatic selectivity with light-driven radical intermediates, provides a transformative route to such reactivity, supporting a range of new biotransformations including amino acid synthesis, multicomponent couplings, and cycloadditions[3,10,11] These transformations leverage both natural and synthetic photoactive elements, such as flavin cofactors, chemical photocatalysts, and photoactive non-canonical amino acids (**Fig. 1a**) [3,11-21]. Despite this promise, current photoenzymatic platforms face major limitations in scalability due to high enzyme loading (e.g., 2-4 g enzyme/L reaction volume), poor stability, and the need for protein purification. Most prior efforts have focused on expanding reactivity *in vitro* or in whole-cell systems, without addressing their translation to robust and scalable production[3,8,11,21-23]. Overcoming these constraints is essential for realizing the potential of photoenzymatic catalysis in synthetic biology and industrial biotechnology.

Synthetic biology provides a powerful framework for designing and engineering biological systems, enabling the construction of improved and novel enzymes, genetic circuits, and microbial cell factories[24]. This approach has been instrumental in the sustainable production of high-value natural products such as artemisinic acid[25], cannabinoids[26], vinblastine[27,28], and vaccine adjuvant QS-21[29]. To extend biosynthesis beyond natural reactivity, an effective strategy involves integrating *in vitro* new-to-nature enzymatic reactions into *in vivo* biosynthetic pathways, enabling the efficient production of

unnatural high-value compounds. A notable example is the microbial platform recently developed by the Hartwig and Keasling groups, which successfully incorporated unnatural carbene-transfer reactions into biosynthesis[30,31].

Inspired by these advances, here we developed an *in vivo* photobiosynthesis platform by integrating photoenzymatic reactions into living systems, enabling scalable and sustainable photoreactions in microbial organisms. Specifically, we engineered *E. coli* to facilitate photoinduced hydroalkylation, hydroamination, and hydrosulfonylation for diverse unnatural product biosynthesis by co-expressing an ene-reductase photoenzyme with a *de novo* designed olefin biosynthetic pathway and supplementing a radical precursor. Additionally, we incorporated an indole biosynthetic pathway and applied directed evolution to enhance the hydroarylation activity with 4-vinylphenol under blue light, culminating in the complete *de novo* biosynthesis of phenol-indole analogue (DIEP) (**Fig. 1b**). The intracellular environment provides a renewable catalytic system, ensuring sustained enzymatic activity for efficient, light-driven biosynthesis.

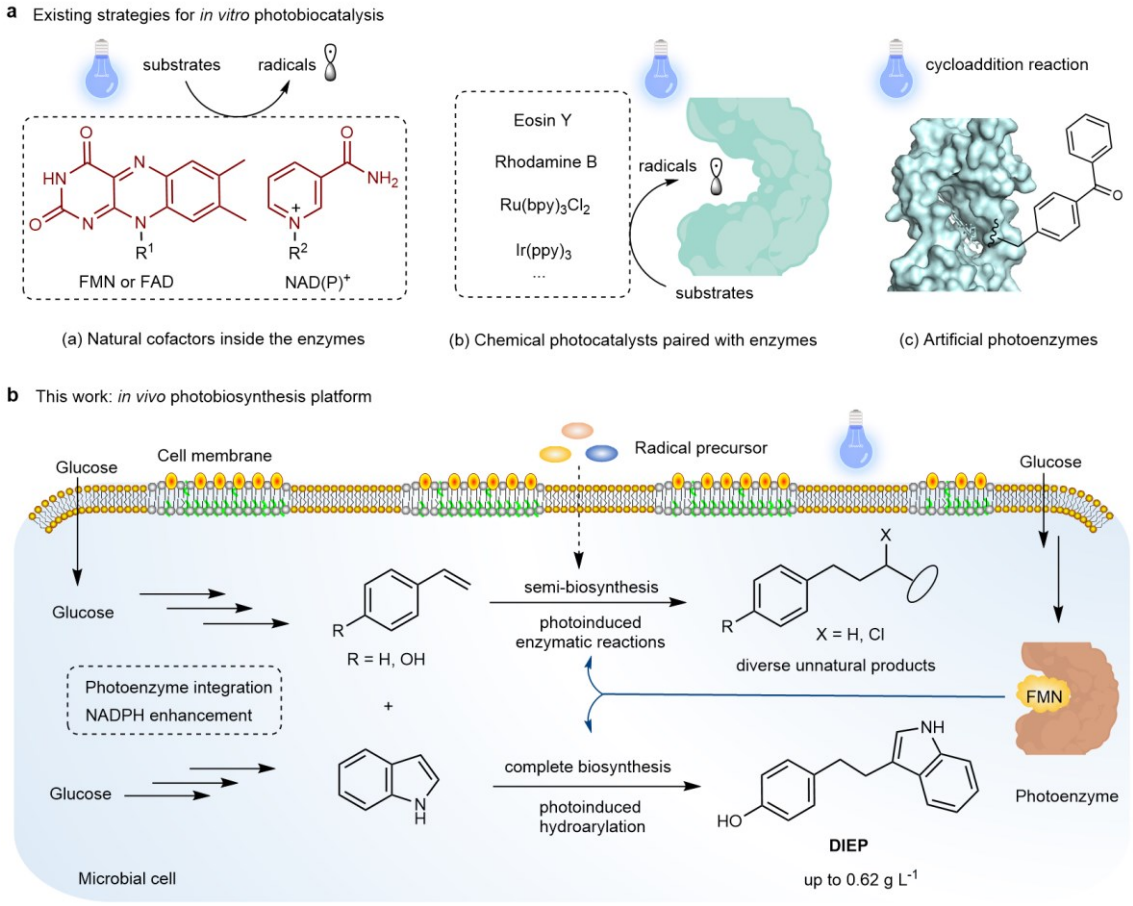

Fig. 1. Integration of *in vitro* new-to-nature enzymatic reactions into *in vivo* biosynthetic pathways. **a**, Existing strategies for developing *in vitro* photobiocatalytic reactions include: a) utilizing photoenzymes containing natural photoactive cofactors; b) coupling enzymes with chemical photocatalysts; c) designing artificial photoenzymes. **b**, Overview of an *in vivo* photobiosynthesis platform that integrates new-to-nature photoenzymatic reactions into the cellular metabolism of *E. coli*. FMN, flavin mononucleotide; FAD, flavin adenine dinucleotide; $NADP^+$, nicotinamide adenine dinucleotide phosphate; bpy, 2,2′-bipyridyl; ppy, 2-phenylpyridine; DIEP, 4-(2-(3a,7a-dihydro-1H-indol-3-yl)ethyl)phenol.

Results

Design and optimization of an *in vivo* photobiosynthesis platform

FMN-dependent ene-reductases exhibit broad substrate promiscuity with diverse radical precursors *in vitro* and have recently been shown to incorporate fluorinated motifs into olefins, addressing the scarcity of natural enzymes capable of synthesizing fluorinated compounds in living organisms[32,33]. Inspired by this, we envisioned integrating photoenzymatic fluorine utilization into microbial biosynthetic pathways, establishing an *in vivo* photobiosynthesis platform to enable microbial production of fluorinated compounds. We selected trifluoroiodoethane (TFIE) as an effective fluorine donor and 4-vinylphenol, a radical acceptor that can be produced in engineered microorganisms. Initial *in vitro* screenings with ene-reductases and their mutants under blue light identified the variant of old yellow enzyme 3 (OYE3_N194Y) as a highly active catalyst, achieving a ~50% yield (**Supplementary Table 1**). We then reconstituted the biosynthetic pathway for 4-vinylphenol in *E. coli* BL21(DE3) by overexpressing the required genes (*palY*, *padA*), along with tyrosine biosynthesis-enhancing genes (*tktA*, *aroF*, *ppsA*, *tyrA*) to enable glucose-to-4-vinylphenol conversion[34] (**Supplementary Figs. 1 and 2**). Under flask fermentation conditions, the engineered photobiosynthesis strain 1 (PBS1) achieved a 4-vinylphenol titre of 129 mg L^{-1} after 48 h in Luria-Bertani (LB) medium. Next, we incorporated the photoenzyme (OYE3_N194Y) expression pathway into the *E. coli* strains harboring the 4-vinylphenol producing pathway (**Figs. 2a and 2b**). For the initial investigation, we developed PBS6, expressing only the photoenzyme and substrate synthesis pathways. Under blue-light irradiation and in an oxygen-free environment, fermentation with TFIE resulted in a 4-(4,4,4-trifluorobutyl) phenol (TFBP) product titre of 2.14 mg L^{-1}. In contrast, no TFBP production was observed in the control strain PBS4, which lacks substrate production, and low TFBP production (0.97 mg L^{-1}) was detected in PBS5 without photoenzyme overexpression, which may be attributed to endogenous background enzymes in *E. coli* BL21(DE3) that exhibit weak catalytic activity (**Fig. 2c, Supplementary Fig. 3**).

NADPH serves as the key cofactor for FMNH regeneration in enzymatic hydroalkylation. To enhance cellular NADPH levels, a set of endogenous (glucose-6-phosphate dehydrogenase, ZWF; membrane-bound transhydrogenase, PntAB; soluble transhydrogenase, UdhA; isocitrate dehydrogenase, ICD) and heterologous (glucose dehydrogenase, GDH; NADH kinase, Pos5; NADP-dependent glyceraldehyde-3-phosphate dehydrogenase, GapC; phosphite dehydrogenase, PTDH; formate dehydrogenases, FDH) NADPH-generating enzymes previously reported were targeted for overexpression[35]. We found that GDH overexpression (in PBS7) and ICD overexpression (in PBS8) improved the TFBP titre by 2.73-fold (7.93 mg L^{-1} vs. 2.14 mg L^{-1}) and 1.41-fold (5.15 mg L^{-1} vs. 2.14 mg L^{-1}), respectively (**Supplementary Figs. 4a-4c**). Additionally, we evaluated the effect of co-expressing GDH and ICD. However, the TFBP titres in the co-expression strains PBS16 and PBS17 were lower than those observed in strains expressing GDH (PBS7) or ICD (PBS8) individually (7.93 mg L^{-1} vs. 5.74 mg L^{-1}; 5.15 mg L^{-1} vs. 3.92 mg L^{-1}, respectively). Further optimization of photoenzyme and NADPH-generating enzyme expression was achieved by regulating the promoter strength. Compared to constructs utilizing strong promoters T7, a combination of the Trc promoter (strong) for the photoenzyme and the Lac promoter (weak) for NADPH generation resulted in a notable improvement in TFBP production (13.78 mg L^{-1} vs. 7.93 mg L^{-1} for GDH and 11.41 mg L^{-1} vs. 5.15 mg L^{-1} for ICD) in PBS24 and PBS25, respectively (**Supplementary Fig. 4d**). To evaluate the effect of radical precursor availability, TFIE concentrations were varied from 1 mM to 40 mM, with an optimal TFBP titre observed at 10 mM both in PBS24 and PBS25 (**Supplementary Fig. 5**). We further evaluated

substrate supply and photoenzyme production by adjusting the plasmid origin of replication to regulate gene copy numbers[36]. TFBP production was significantly improved compared to the initial strain (PBS6) (41.41 mg L^{-1} vs. 2.14 mg L^{-1} and 35.44 mg L^{-1} vs. 2.14 mg L^{-1}) when a medium-copy plasmid (pBR322 ori, ~40 copies) was used for substrate production and a high-copy plasmid (pRSF ori, >100 copies) was employed for photoenzyme production in PBS28 and PBS29, respectively (**Fig. 2c, Supplementary Fig. 4e**). Additionally, a comparative analysis was conducted to evaluate the catalytic efficiency between strains co-expressing the substrate pathway and photoenzyme, and those expressing only the photoenzyme with exogenous supplementation of 4-vinylphenol. The results showed that TFBP titres were significantly lower in these strains lacking substrate production (17.24 mg L^{-1} in PBS30 and 15.66 mg L^{-1} in PBS31) despite exogenous 4-vinylphenol addition, likely due to limited membrane permeability. In contrast, intracellular biosynthesis ensures continuous and localized substrate availability near the photoenzyme, thereby enhancing catalytic efficiency (**Supplementary Fig. 4f**).

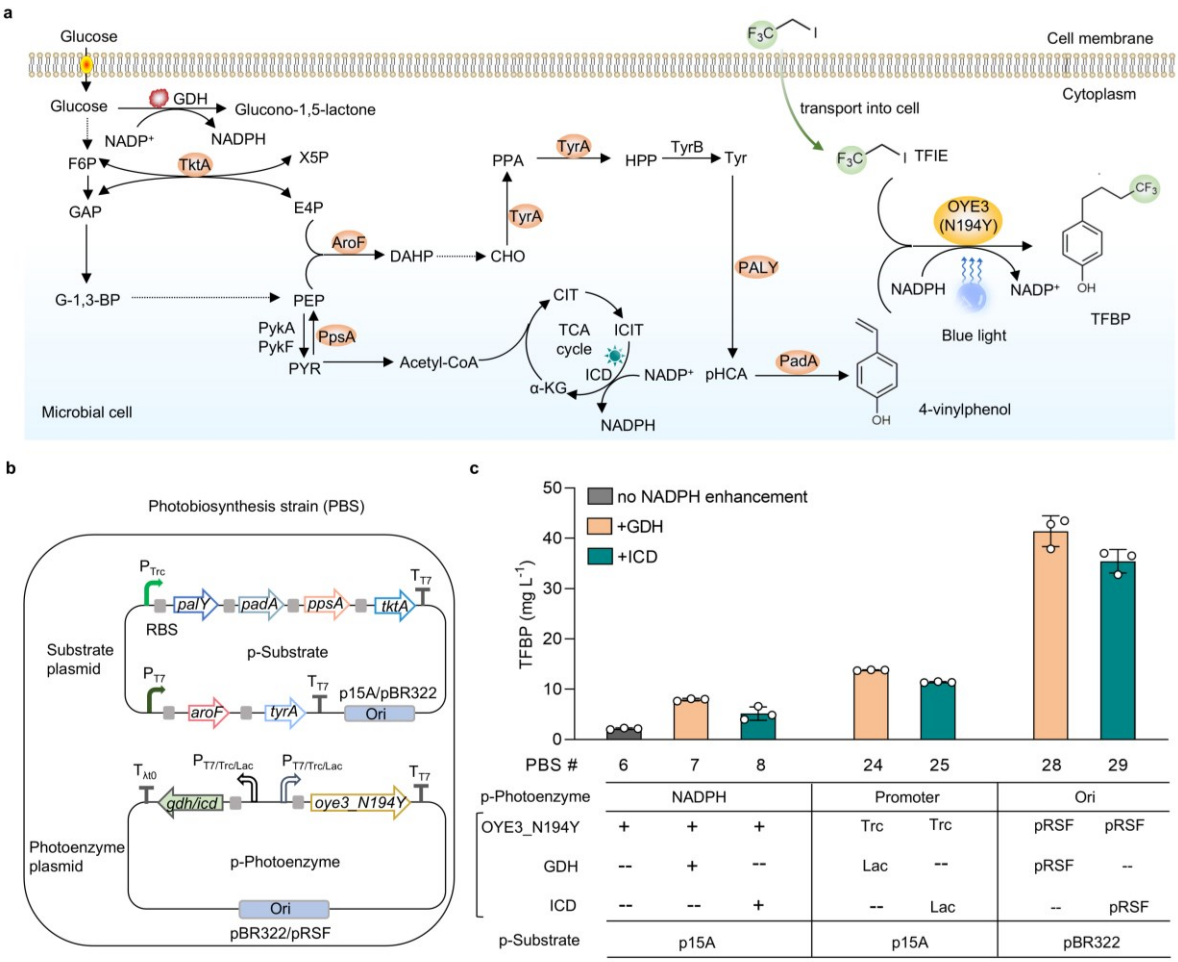

Fig. 2. Design and optimization of an *in vivo* photobiosynthesis platform. **a**, Design of a photobiosynthetic microbial cell by integrating olefin substrate biosynthetic enzymes (orange), photoenzyme (yellow), and NADPH-generating enzymes (GDH and ICD). Dotted arrows represent multistep catalytic processes. **b**, Construction of photobiosynthesis strains. p-Substrate contains substrate (4-vinylphenol) biosynthetic enzymes. p-Photoenzyme contains photoenzyme and GDH or ICD. **c**, Optimization of photobiosynthesis platform, including the evaluation of NADPH-enhancing

systems for photobiosynthesis in microorganisms, combinatorial optimization of promoters for the overexpression of photoenzyme and GDH or ICD, and balancing substrate supply and photoenzyme production by adjusting plasmid origin of replication. OYE3, old yellow enzyme 3 from *Saccharomyces cerevisiae*; Single-letter abbreviations for the amino acid residues: N-Asn (Asparagine), Y-Tyr (Tyrosine); GDH, glucose dehydrogenase; ICD, isocitrate dehydrogenase; TktA, transketolase; AroF, 3-deoxy-D-arabino-heptulosonate-7-phosphate (DAHP) synthetase; PpsA, phosphoenolpyruvate synthase; TyrA, tyrosine synthase; PALY, phenylalanine ammonia lyase from *Rhodotorula toruloides*; PadA, decarboxylase from *Lactiplantibacillus plantarum*; F6P, fructose 6-phosphate; GAP, glyceraldehyde 3-phosphate; PEP, phosphoenolpyruvate; PYR, pyruvate; CIT, citrate; ICIT, isocitrate; X5P, xylulose 5-phosphate; E4P, erythrose 4-phosphate; CHO, chorismate; PPA, prephenate; HPP, 4-hydroxyphenylacetone; pHCA, *p*-hydroxy-cinnamic acid; TFIE, trifluoroiodoethane; TFBP, 4-(4,4,4-trifluorobutyl)phenol; RBS, ribosome binding site; P_{T7}, T7 promoter; P_{trc}, trc promoter; P_{lac}, lac promoter; T_{T7}, T7 terminator; $T_{\lambda0}$, λ0 terminator; ori, origin of replication; TCA, tricarboxylic acid; PBS, photobiosynthesis strain. The data represent three independent experiments and are presented as the mean ± s.d.

Expanding the scope to various photoenzymatic reactions

To broaden the applicability of the *in vivo* photobiosynthesis platform, various photoenzymatic transformations were explored. For an additional olefin substrate, we reconstituted a styrene biosynthetic pathway in *E. coli* by overexpressing the required genes (*pal2* and *fdc1*) along with the precursor (phenylalanine) biosynthetic genes (*tktA*, *ppsA*, *aroF*, and *pheA*)[37] (**Supplementary Figs. 6 and 7)**. Under flask fermentation conditions, the engineered strain (PBS32) produced 75.17 mg L^{-1} of styrene after 72 h in LB medium. The most efficient photobiosynthesis platform was then evaluated for its compatibility with various enzymatic hydroalkylation[12,38-41], hydroamination[42], and hydrosulfonylation[41] reactions (**Fig. 3a**). The biologically synthesized styrene or 4-vinylphenol underwent radical-mediated transformations with different precursors, including piperidin-1-yl benzoate, 2-bromo-1-phenylethanone, 4-methylbenzene-1-sulfonyl chloride, 4-(bromomethyl)pyridine, and 2,2-dichloro-1-(pyrrolidin-1-yl)ethanone, yielding unnatural products with titres ranging from 4.5 mg L^{-1} to 98.3 mg L^{-1} (**Figs. 3b-3f, Supplementary Figs. 8-12**). The photobiosynthetic cells demonstrated high compatibility with the azaarene-type photoenzymatic radical reaction, achieving a titre of 98.3 mg L^{-1} (**Fig. 3e**). Furthermore, the results revealed comparable enantioselectivities of the asymmetric photoenzymatic reaction for α-chloroamide synthesis both *in vivo* and *in vitro* (86% vs. 91% *ee*) (**Fig. 3f, Supplementary Fig. 13**). The reduced stereo-selectivity may be attributed to endogenous enzymes in *E. coli* catalyzing the reaction with minimal catalytic activity (**Supplementary Fig. 14**).

We next aimed to explore the feasibility of scaling up highly challenging photoenzymatic reactions, including those requiring precise light sources and strict anaerobic conditions, using a microbial platform. To this end, we initially conducted photobiosynthetic fermentation in microbioreactors. Compared with whole-cell catalysis using resting cells—particularly regarding cell recycling efficiency and sustained cofactor turnover, a key advantage of fermentation systems lies in the metabolically active state of cells, which enables continuous endogenous cofactor regeneration, enzyme production, and substrate replenishment through engineered metabolic pathways. In flavin-dependent photoenzymatic catalysis, the exclusion of oxygen is critical due to its dual inhibitory roles: molecular oxygen rapidly quenches alkyl radical intermediates, thereby suppressing productive coupling; and under light irradiation, oxygen oxidizes the reduced FMN cofactor ($FMNH^-$), depleting the system's reductive

capacity and hindering radical generation via single-electron transfer. These effects severely limit catalytic efficiency. To maintain both radical stability and enzymatic activity, photobiosynthesis must therefore proceed under strictly anaerobic conditions. Therefore, a dual-phase fed-batch fermentation process was implemented: Phase I involved substrate production under aerobic conditions, while Phase II initiated photobiosynthesis under blue light in a nitrogen environment. Utilizing this strategy, we evaluated the scale-up of representative photoenzymatic reactions to produce fluorinated-, azaarene-, and α-chloroamide-based unnatural products (TFBP, PPPy, CPPB) through glucose feeding. Monitoring the fermentation process revealed improvements in product titres: TFBP was increased by 1.56-fold (64.65 mg L^{-1}), PPPy by 1.76-fold (172.04 mg L^{-1}), and CPPB by 3.46-fold (38.03 mg L^{-1}) (**Fig. 3g, Supplementary Fig. 15**). These results demonstrated the potential for scaling up photoenzymatic reactions under automated and precise control of conditions such as dissolved oxygen (DO), nitrogen flow, and agitation in bioreactors.

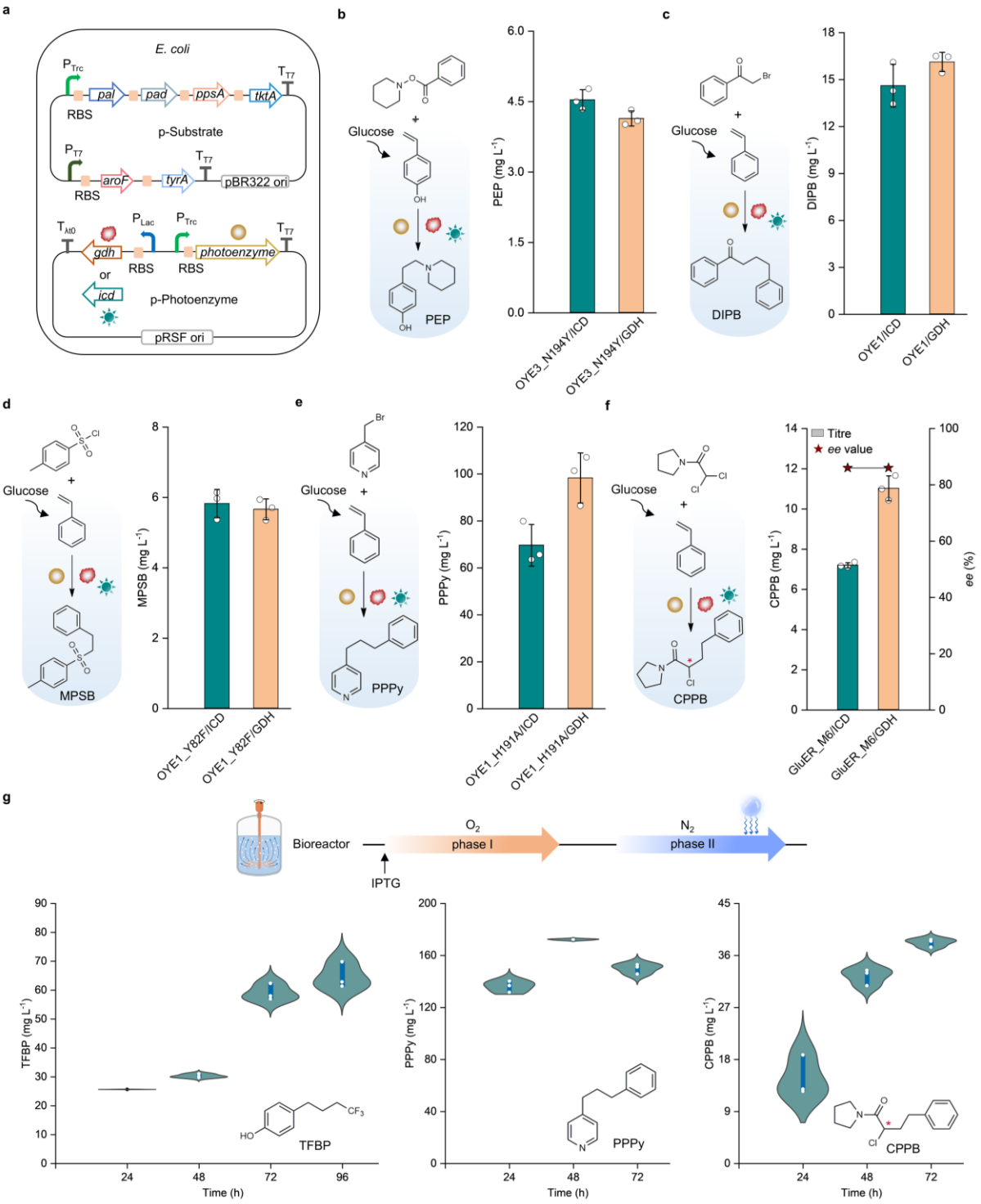

Fig. 3. Expanding the scope of the *in vivo* photobiosynthesis platform. **a**, Schematic of a general strategy for photobiosynthesis with a diverse range of photoenzymatic reactions. **b-f**, Incorporation of photoenzymatic reactions triggered by radical precursors, including piperidin-1-yl benzoate, 2-bromo-1-phenylethanone, 4-methylbenzene-1-sulfonyl chloride, 4-(bromomethyl)pyridine, and 2,2-dichloro-1-(pyrrolidin-1-yl)ethanone, within microbial cells. **g**, Evaluation of the scalability of photoenzymatic reactions in the microbial platform through bioreactor fermentation. The data represent three independent experiments and are presented as the mean ± s.d. FG, function group; LG, leaving group; PEP, 4-(2-(piperidin-1-yl)ethyl)phenol; DIPB, 1,4-diphenylbutan-1-one; MPSB, 1-methyl-4-

(phenethylsulfonyl)benzene; PPPy, 4-(3-phenylpropyl) pyridine; CPPB, 2-chloro-4-phenyl-1-(pyrrolidin-1-yl)butan-1-one; IPTG, isopropyl-β-D-thiogalactoside; OYE3, old yellow enzyme 3 from *S. cerevisiae*; OYE1, old yellow enzyme 1 from *S. patorianus*; GluER, the ene-reductase from *Gluconobacter oxydans*. OYE3_N194Y, OYE1, OYE1_Y82F, OYE1_H191A, and GluER_M6 were the optimal photoenzymes used for the corresponding reactions. *pal*: *palY* for 4-vinylphenol production and *pal*2 for styrene production; *pad*: *pad*A for 4-vinylphenol production and *fdc* for styrene production. *The enantioselective excess (*ee*) value was determined by isolating products from *E. coli* fermentation broth using chiral gas chromatography (GC).

Complete integration of a photoenzymatic reaction into cellular metabolism

Building on the successful incorporation of photoenzymatic reactions into microbial cells via radical precursor feeding, we sought to achieve complete pathway integration by reconstituting the biosynthetic pathways for the radical precursor, substrate, and photoenzyme in *E. coli*. Indole is a structural motif frequently found in pharmaceutically active molecules, contributing to diverse biological activities[43]. Inspired by a recent work on redox-neutral radical hydroarylation[44], a model photoenzymatic route was designed, wherein indole couples with 4-vinylphenol, catalyzed by a photoenzyme in microbial cells, thereby expanding the biosynthetic strategy for indole-derived compounds. In *E. coli*, indole biosynthesis occurs via tryptophanase, which reversibly converts tryptophan into indole, pyruvate, and ammonia within the tryptophan metabolic pathway[45] (**Supplementary Figs. 16 and 17**). By encoding the *tnaA* gene in *E. coli* strains, indole production was achieved with a titre of 57.13 mg L^{-1} in PBS41 under flask condition. To construct the initial complete photobiosynthesis strain, *tnaA* was co-overexpressed with the 4-vinylphenol and OYE1 biosynthetic pathways (**Fig. 4a and 4b**). The strain (PBS42) was cultivated under blue light irradiation in an oxygen-free environment, enabling the complete biosynthesis of unnatural product DIEP. After 48 h of fermentation in LB medium, DIEP was detected, achieving a titre of 0.71 mg L^{-1} (**Fig. 4c**).

Previous mechanistic investigations revealed that the free cofactor riboflavin 5-monophosphate sodium salt (FMN-Na) enhanced the yield of photoinduced hydroarylation *in vitro*[44]. A concentration-dependent analysis showed that increasing FMN-Na to 1 mM significantly improved DIEP production (5.42 mg L^{-1}), while concentrations exceeding 1 mM provided no further enhancement (**Fig. 4c, Supplementary Fig. 18**). To further optimize enzyme expression levels, plasmid origins of replication were adjusted. DIEP production was increased in strain PBS43 when a high-copy plasmid (pRSF ori, >100 copies) was used for photoenzyme expression, compared to strain PBS42, which utilized a medium-copy plasmid (pBR322 ori, ~40) (17.82 mg L^{-1} vs. 5.42 mg L^{-1}). In both strains, the 4-vinylphenol biosynthetic pathway was maintained on medium-copy plasmids, while the indole biosynthetic enzyme was encoded on low-copy plasmids to optimize metabolic flux and minimize cellular burden (**Fig. 4c**). To further enhance titres, protein engineering was applied to improve the activity of the photoenzyme old yellow enzyme 1 (OYE1) for indole and 4-vinylphenol *in vivo*. A mutant library comprised of 95 OYE1 variants with substitutions near the active site was generated and screened using a high-throughput whole-cell based screening protocol. The workflow involved parallel cultivation, reaction, and product analysis in multi-well plates. After protein expression in 24-deep-well plates, concentrated cells were transferred to 96-deep-well plates for photobiocatalytic reactions under anaerobic illumination. Products were extracted post-reaction and analyzed by LC-MS, enabling rapid screening of engineered variants. After three rounds of targeted mutagenesis and one round of gene

recombination by the staggered extension process (StEP)[46], we obtained an OYE1 variant Y82G/T37Q/W116A/H191S with the highest catalytic efficiency in whole-cell photoenzymatic reactions, demonstrating a 12.7-fold activity improvement compared to wild type OYE1 (OYE1_WT) (**Supplementary Table 6**). Subsequently, photobiosynthetic strains expressing OYE1 variants (Y82G in PBS44, Y82G/T37Q in PBS45, and Y82G/T37Q/W116A/H191S in PBS46) were constructed and cultured under blue-light fermentation, where the observed titres aligned with whole-cell based screening results (**Supplementary Fig. 20**). The PBS46 strain, harboring the Y82G/T37Q/W116A/H191S variant, achieved a high titre of 94.06 mg L^{-1}, representing a 4.28-fold improvement compared to OYE1_WT (17.82 mg L^{-1}) (**Fig. 4c**).

To further enhance fermentation yields, fed-batch fermentation in a bioreactor was conducted, providing better O_2 availability and pH control. The best-performing strain (PBS46) was evaluated for DIEP production using glucose as the carbon source, demonstrating further optimization of microbial photobiosynthesis under controlled conditions. To characterize product formation dynamics, a dual-phase fermentation profile was established, comprising three distinct stages: Stage 1: The strain was cultured under O_2 until the substrate accumulation reached its target peak, after which O_2 was replaced with N_2; Stage 2: N_2 was maintained for approximately 10 hours without blue light to deplete residual O_2 in the medium and cells; Stage 3: Photobiosynthesis was initiated with the introduction of blue light (**Supplementary Fig. 21a**). Throughout the process, product formation, glucose and substrate consumption and accumulation, and cell growth were monitored. After the substrate reached its peak accumulation and O_2 was deplete, photobiosynthesis was initiated, leading to the production of 0.34 g L^{-1} DIEP at 191 h (**Supplementary Figs. 21b and 22a**). Next, we assessed the optimal ratio of indole to 4-vinylphenol under fermentation conditions. The results showed that the highest yield was achieved when the substrate ratio ranged from 1:1 to 1:2 (**Supplementary Fig. 23**). Based on this finding, we optimized the timing of light exposure initiation at substrate accumulations within this ratio to maintain maximum enzyme catalytic activity, achieving a product titre of 0.36 g L^{-1} (**Supplementary Fig. 21c and 22b**). Throughout the fermentation process, indole production was suppressed as 4-vinylphenol accumulated, likely attributed to the competitive inhibition from the shared amino acid precursor, the same expression regulation system induced by IPTG, and the biotoxicity of 4-vinylphenol toward *E. coli* BL21(DE3), inhibiting the physiological metabolism of the strain and reducing synthesis efficiency[47]. To overcome the constraints, we implemented two separate sequential induction systems, with arabinose initiating indole production at the initial stage, followed by IPTG induction for 4-vinylphenol and photoenzyme expression. The results revealed that the production of DIEP was significantly improved, reaching a titre of 0.62 g L^{-1}, a 33.79-fold improvement compared to the parent strain PBS43 (17.82 mg L^{-1}) (**Fig. 4d and Supplementary Fig. 22c**). We also evaluated DIEP production in M9 minimal medium. Although the titre (0.2 g L^{-1}) was lower than in LB rich medium, it still represented a 280.69-fold improvement compared to the parent strain, demonstrating scalability in bioreactor conditions. In addition, we investigated the effect of varying light intensity (25%, 50%, 75%, and 100%) on DIEP production. The results showed that higher light intensities led to increased titres, suggesting that light diffusion within the bioreactor is a key factor and that sufficient illumination is essential for high production (**Supplementary Fig. 24**). Furthermore, live/dead staining analysis revealed a decrease in cell viability during the photoreaction, with live cell ratios ranging from 60% to 80%. These findings suggest that prolonged exposure to photoreaction conditions can lead to partial cell damage, which may negatively affect product generation (**Supplementary Fig. 25**).

In addition, the bioactivity evaluation of DIEP revealed its broad-spectrum antimicrobial activity

against gram-negative and gram-positive bacteria, including the multidrug-resistant pathogens such as Methicillin-resistant *Staphylococcus aureus* (MRSA), vancomycin-resistant *Enterococcus faecium* U503 (VRE) and *Acinetobacter baumannii*, as well as fungi, with low minimum inhibitory concentration (MIC) values ranging from 16 to 32 μg mL^{-1} (**Fig. 4e, Supplementary Figs. 26 and 27**). Notably, DIEP also exhibited antibacterial activity against *E. coli*, and as demonstrated in our antimicrobial assays (**Supplementary Fig. 28**), cell growth was significantly inhibited when the concentration exceeded 0.5 g L^{-1}. Therefore, the accumulation of DIEP during fermentation could potentially inhibit cell growth and limit its production titre.

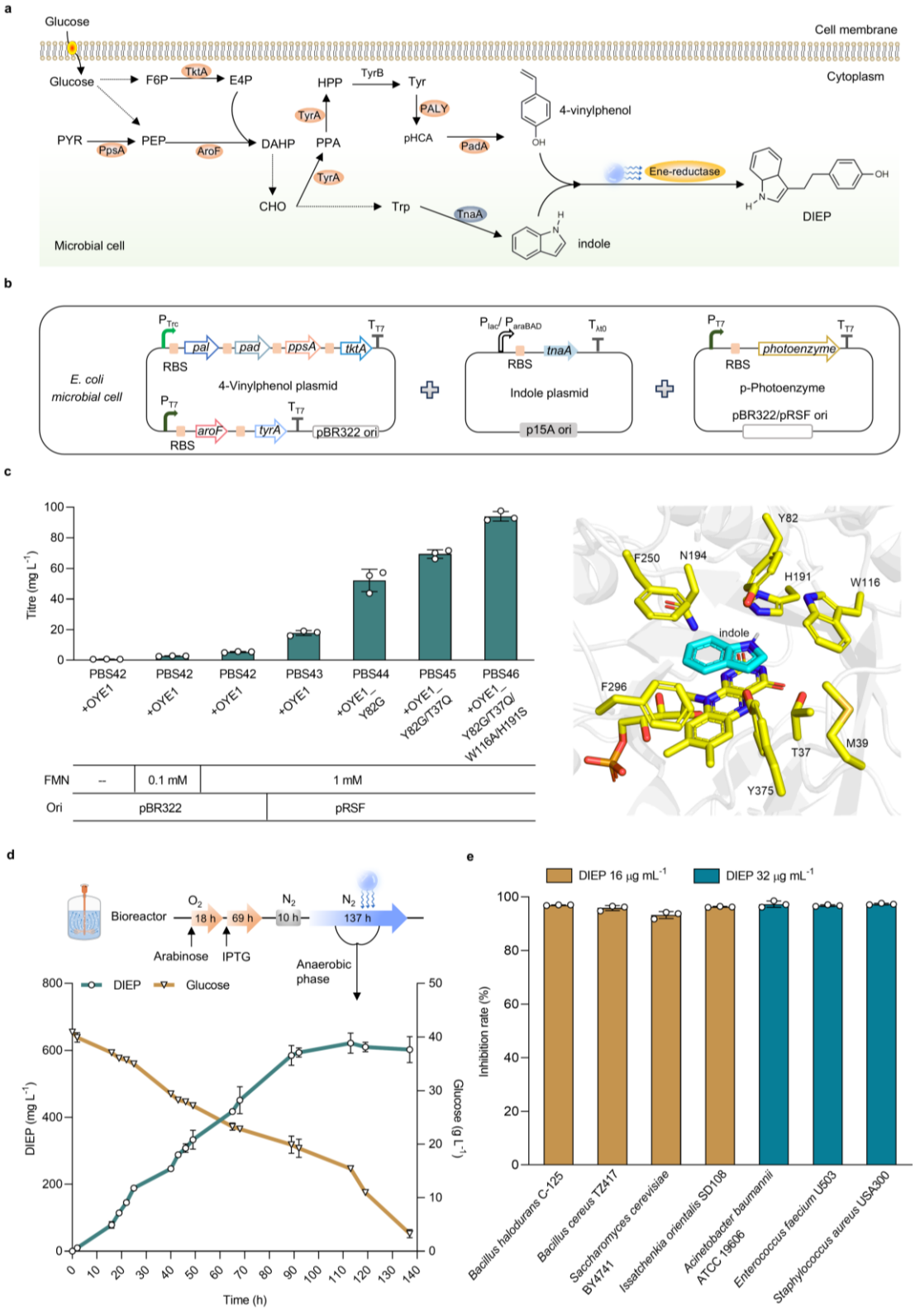

Fig. 4. Coupling photoenzymatic reaction into metabolic networks. **a**, Schematic of engineering a photobiosynthetic strain with the substrates and enzymes made by the cells. Dotted arrows represent multistep catalytic processes. **b**, Construction of complete photobiosynthesis strains. **c**, Optimization of DIEP production by regulating FMN-Na supply and gene copy numbers and applying protein engineering. Strain PBS42 used a medium-copy plasmid (pBR322 ori, ~40 copies) for photoenzyme

expression, while PBS43-PBS46 employed a high-copy plasmid (pRSF ori, >100 copies). Both strains maintained the 4-vinylphenol pathway on medium-copy plasmids and indole biosynthetic enzymes on low-copy plasmids (p15A ori, ~10 copies). Modeled structure of OYE1 was conducted using AutoDock Vina[48]. **d**, DIEP production from glucose in bioreactor fermentation. The data presented corresponds to the anaerobic phase under blue light. **e**, Bioactivity evaluation of DIEP. Data of **d** are presented as mean ± s.d. of biological duplicates ($n = 2$), and data of **c** and **e** are presented as mean ± s.d. of biological triplicates ($n = 3$). DIEP, 4-(2-(3a,7a-dihydro-1H-indol-3-yl)ethyl)phenol; FMN-Na, riboflavin 5-monophosphate sodium salt; OYE1, old yellow enzyme 1 from *S. patorianus*; TktA, transketolase; AroF, 3-deoxy-D-arabino-heptulosonate-7-phosphate (DAHP) synthetase; PpsA, phosphoenolpyruvate synthase; TyrA, tyrosine synthase; PALY, phenylalanine ammonia lyase from *Rhodotorula toruloides*; PadA, decarboxylase from *Lactiplantibacillus plantarum*; F6P, fructose 6-phosphate; PEP, phosphoenolpyruvate; PYR, pyruvate; E4P, erythrose 4-phosphate; CHO, chorismate; PPA, prephenate; HPP, 4-hydroxyphenylacetone; pHCA, *p*-hydroxy-cinnamic acid; Tyr, tyrosine; Trp, tryptophan; TnaA, tryptophanase. Single-letter abbreviations for the amino acid residues: Y, Tyr; G, Gly; T, Thr; Q, Gln; W, Trp; A, Ala; H, His; S, Ser.

Conclusions

This study demonstrates the successful integration of photoenzymatic catalysis into microbial biosynthesis, establishing a scalable *in vivo* photobiosynthetic platform that enables light-driven enzymatic transformations in living cells. By incorporating FMN-dependent ene-reductases into engineered *E. coli*, this system facilitates the semi-biosynthesis of diverse unnatural products and achieves *de novo* complete biosynthesis of DIEP through simultaneous expression of photoenzyme as well as reconstitution of radical precursor and substrate biosynthetic pathways within microbial organisms. This work establishes a rational and programmable framework for microbial photobiosynthesis, expanding the synthetic capabilities of biological systems beyond nature's constraints. These findings have laid the foundation for sustainable biomanufacturing, offering opportunities for production of high-value pharmaceuticals, bioactive molecules, and complex natural products through light-driven enzymatic transformations in living systems.

Methods

Materials and reagents. Polymerase chain reaction (PCR) amplification of DNA fragments for plasmid construction was performed using PrimeSTAR® Max DNA Polymerase (R045B, TaKaRa, Kyoto, Japan). PCR primers were synthesized by Integrated DNA Technologies (IDT, Coralville, IA, USA). All amplified fragments were purified using the D2000 Gel & PCR clean up kit (D2000-00, Omega Bio-Tek, GA, USA). NEBuilder® HiFi DNA Assembly Master Mix kits were purchased from New England Biolabs (E2621S, NEB, Ipswich, MA, USA). All plasmids were extracted using the QIAprep® Miniprep kit (27106, QIAGEN, Hilden, Germany). All commercial organic reagents were purchased from Sigma-Aldrich (Louis, MO, USA). Chemically synthesized standards have a purity of at least 95%. Detailed synthesis methods are provided in the Supplementary Information.

Plasmid and strain construction. Plasmids, strains, and oligonucleotide primers used in this study are listed in **Supplementary Table 2**, **3** and **5**, respectively. Fragments used in plasmid construction were amplified by PCR using the corresponding templates and primers and joined using the NEBuilder® HiFi DNA Assembly Master Mix kit (**Supplementary Table 4**). Nucleotide and amino acid sequences of enzymes are listed in Supplementary Information (**Supplementary Table 7**). *E. coli* NEB5a used for cloning and plasmid propagation was cultured on selective LA plates (LB with 1.6% agar) or in selective LB medium. Kanamycin, ampicillin, and chloramphenicol were supplemented at 50, 100, and 34 μg mL^{-1}, respectively. All plasmids were verified by digesting with the appropriate restriction enzymes and sequenced. Recombinant *E. coli* BL21(DE3) cells harboring relevant plasmids (**Supplementary Table 3**) were constructed for product production.

Biosynthetic pathways reconstitution. To overproduce 4-vinylphenol, styrene, and indole, plasmids containing the corresponding biosynthetic genes were constructed (**Supplementary Table 3**). The *aroF*, *tyrA*, *pheA*, *ppsA*, *tktA*, and *tnaA* genes were amplified from *E. coli* MG1655 genomic DNA. The heterologous genes *palY* from *Rhodotorula toruloides*, *padA* from *Lactiplantibacillus plantarum*, *pal2* from *Arabidopsis thaliana*, and *fdc1* from *Saccharomyces cerevisiae* were codon-optimized for *E. coli* expression and synthesized by Twist Bioscience. For 4-vinylphenol production, gene fragments *aroF* and *tyrA* under T7 promoter regulation, along with *palY*, *padA*, *ppsA*, and *tktA* under Trc promoter regulation, were cloned into the pACYC and pET30a(+) vectors using HiFi DNA assembly to generate plasmids pYJ749 and pYJ751, respectively. For styrene production, *aroF* and *pheA* under T7 promoter regulation, together with *pal2*, *fdc1*, *ppsA*, and *tktA* under Trc promoter regulation, were cloned into the pET30a(+) vector to construct plasmid pYJ753. For indole production, the *tnaA* gene fragment was cloned under the control of either the Lac promoter or araBAD promoter into the pACYC vector using HiFi DNA assembly, resulting in plasmids pYJ755 and pYJ783, respectively. The recombinant *E. coli* BL21(DE3) strains were constructed by transforming the respective plasmids.

Shake-flask fermentation. Plasmids carrying genes encoding the biosynthetic pathways for 4-vinylphenol, styrene, and indole production were transformed into *E. coli* BL21(DE3) competent cells. Single colonies were cultured overnight in 5 mL LB medium with appropriate antibiotics at 37 °C and 250 rpm to obtain the seed culture. For shake-flask fermentation, the seed culture was inoculated at 1% (v/v) into 50 mL LB medium with appropriate antibiotics in a 250 mL flask and incubated at 37 °C and 220 rpm. When the OD600 reached 0.6-0.8, cells were induced with 0.1 mM IPTG and cultured at 25 °C and 220 rpm. Cell cultures including both the medium and the cell pellets (1 mL) were collected at 24 h, 48 h, and 72 h post-induction for analysis. For GC quantification, dodecane (10 mM, 50 μL) was

added, and cell cultures were extracted with 1 mL ethyl acetate by vortexing. The product titre was determined using GC based on a calibration curve established with pure standards. Three biological replicates were performed from independent fermentations.

Photobiosynthesis in vials. Photobiosynthetic strains carrying biosynthetic pathways for substrate and photoenzyme production were constructed by transforming plasmids into *E. coli* BL21(DE3) competent cells. Single colonies were cultured overnight in 5 mL LB medium with appropriate antibiotics at 37 °C and 250 rpm to obtain the seed culture. For initial substrate accumulation under aerobic conditions, shake-flask fermentation was performed by inoculating the seed culture (1%, v/v) into 50 mL LB medium with appropriate antibiotics in a 250 mL flask and incubating at 37 °C and 220 rpm. When the OD600 reached 0.6-0.8, cells were induced with 0.1 mM IPTG and cultured at 25 °C and 220 rpm for an additional 48 h. Following fermentation, 20 mL of culture broth was transferred into a 40 mL glass vial (23188, Sigma-Aldrich, Louis, MO, USA) inside a nitrogen-filled glovebox, supplemented with 20 g L^{-1} glucose, 10 mM radical precursors, or 1 mM FMN-Na for complete photobiosynthesis. The culture broth was then placed in a photobiosynthesis setup with stirring and illuminated at 25 °C for 48 h using a Kessil PR160 Rig equipped with a Fan Kit and four 40 W, 440 nm blue LEDs (**Supplementary Fig. 31**). After illumination, the fermentation broth was extracted with 20 mL ethyl acetate, supplemented with an internal standard-either dodecane (10 mM, 50 μL) for GC-MS quantification or 2-hydroxyindole for HR-LC/MS analysis. The organic extracts were dried over anhydrous $MgSO_4$, filtered to remove the drying agent, and concentrated. The resulting residue was then resuspended in 300 μL of ethyl acetate for GC-MS analysis or 300 μL of methanol for HR-LC/MS determination.

Construction of photoenzyme variants. For targeted mutagenesis, three PCR fragments were assembled using HiFi assembly. Mutagenesis primers were ordered in 96-deep well plates from IDT. Plasmids serving as PCR templates were linearized with restriction enzymes, purified using a PCR cleanup kit, and stored for further use. The PCR fragments contained 27-40 bp overlapping sequences. The vector backbone PCR was treated with *Dpn*I (37 °C for 4 hours, followed by overnight incubation at room temperature), purified, and stored at -20 °C. PCR for forward and reverse fragments was performed separately in 96-well plates, followed by *Dpn*I treatment. Q5 DNA polymerase (NEB #M0491) was used for PCR. The HiFi assembly reaction (15 μL) was set up using 30 ng of purified vector backbone PCR, 1.25 μL each of *Dpn*I-treated forward and reverse PCR products, and 7.5 μL of HiFi master mix. Homemade competent DH5α cells in a 96-well plate (Bio-Rad #HSS9641) were transformed with 5 μL of the HiFi reaction by heat shock (30 seconds), followed by 1-hour cell growth in 150 μL SOC medium. The resulting cultures were plated on 8-well omnitray plates (120 μL per well) supplemented with kanamycin (50 μg mL^{-1}) and incubated overnight at 37 °C. Colonies were picked and grown overnight at 37 °C in a 96-deep well plate containing 1 mL of Terrific Broth (TB) with kanamycin. Minipreps were performed using the PureLink Pro Quick96 Plasmid Purification Kit (Invitrogen #K211004A), and plasmid DNA from selected mutants was sent for sequencing. The miniprep DNA was then used to transform competent BL21(DE3) cells in a 96-well plate for subsequent whole-cell reactions.

For staggered extension process (StEP) recombination[46], plasmids containing enzyme variants with improved activity (Y82G, T37Q, T37A, W116A, N194A, M39Y, H191S, M39Q, H191Y, Y375E, and Y375L) were combined in equal concentrations to achieve a final DNA mixture concentration of ≥ 60 ng μL^{-1}. A master mix (144 μL total) for the first PCR of StEP was prepared as follows: 60 ng μL^{-1} Template (59.98 μL), 1 μM Forward primer (7.2 μL), 1 μM Reverse primer (7.2 μL), 10 mM dNTPs

(2.88 μL), 10× *Taq* buffer (14.4 μL), 5 U/μL *Taq* DNA polymerase (2.38 μL), and PCR grade H_2O (49.97 μL). This master mix was aliquoted into six 20 μL reactions, each subjected to different elongation temperatures (50-72 °C) to determine the optimal conditions. Temperature profile for the first PCR in the StEP recombination procedure was set up as follows: Initial denaturation, 95 °C-5 min; Denaturation, 95 °C-10 s; Annealing, 55 °C-1 s; Elongation, 50-72 °C-1 s; Final elongation, 72 °C-5 min; Hold, 10 °C-∞. The optimal elongation temperature was determined by analyzing the PCR products on an analytical gel, selecting the reaction with the most discrete band. The selected PCR product was treated with 1 μL *Dpn*I at 37 °C for 1 h to digest the parental template. The protocol to amplify 5 μL of the *Dpn*I digested reaction mixture with Phusion DNA polymerase was set up as follows (100 μL total): Template (5 μL), 10 μM Forward primer (4 μL), 10 μM Reverse primer (4 μL), DMSO (4 μL), 10 mM dNTPs (2 μL), 5× HF buffer (20 μL), 2 U μL^{-1} Phusion DNA polymerase (1 μL), PCR grade H_2O (60 μL). Temperature profile for the second PCR in the StEP recombination procedure was set up as follows: Initial denaturation, 98 °C-30 s; Denaturation, 98 °C-10 s; Annealing, 55 °C-15 s; Elongation, 72 °C-1 min; Final elongation, 72 °C-10 min; Hold, 10 °C-∞. The PCR products were analyzed on a 1% agarose gel, purified using a DNA gel recovery kit, and subsequently used for plasmid construction. The amplified and purified DNA fragments were assembled using HiFi DNA assembly with corresponding vector fragments. Homemade electroporation competent *E. coli* BL21(DE3) cells (60 μL) were transformed with 10 μL of the HiFi reaction using 1 mm cuvettes (Bio-RAD) under the following settings: Voltage-1250, Capacity-25, Resistance-100 Ω. Post-transformation, cells were recovered in 1 mL SOC medium and incubated at 37 °C for 1 h. Transformed cultures were plated on kanamycin (50 μg mL^{-1}) LB agar plates and incubated overnight at 37 °C. Colonies were picked and grown overnight at 37 °C in a 96-deep well plate containing 0.5 mL of LB medium with kanamycin. After incubation, 0.5 mL 40% glycerol was added to each well for storage at -80 °C.

High-throughput whole-cell reactions. The photobiosynthesis strains in a 96-deep well plate were inoculated into fresh LB medium supplemented with 50 μg mL^{-1} kanamycin in a new 96-deep well plate and incubated overnight at 37 °C with shaking at 220 rpm. The overnight seed cultures were then inoculated into a 24-deep well plate (1%, v/v) containing 6 mL TB per well with 50 μg/mL kanamycin and grown at 37 °C with shaking at 200 rpm. Once the OD600 reached 0.4-0.6, the cultures were cooled to 18 °C with continued shaking (200 rpm) for 30 min. Protein expression was induced by adding IPTG to a final concentration of 0.1 mM, followed by incubation at 18 °C with shaking at 200 rpm for 18 h. After measuring OD600, approximately 60 OD600 units of each culture were collected by centrifugation at 3,000 g for 10 min, and the supernatants were discarded. The cell pellets (~100 μL per well) were resuspended in 220 μL M9 buffer inside a nitrogen-filled glovebox and transferred to a 96-deep well plate (DWP-7651-S0-C, STELLAR SCIENTIFIC). The following components were added to each well: 4-vinylphenol (100 mM stock in DMSO, 40 μL), indole (100 mM stock in DMSO, 40 μl), glucose (40% stock in H_2O, 50 μL), and FMN-Na (10 mM stock in H_2O, 50 μL). This resulted in the desired final concentrations, with a total reaction volume of 500 μL and a final cell concentration of OD600 = 120. The 96-deep well plate was sealed with a sticky cover, and the reactions were carried out using a Lumidox® II 96-Well LED Array equipped with an active cooling base. The plate was shaken at 900 rpm using a Deep Well Plate Thermoshaker (Mfr. No. TS-DW USA) at 25 °C for 48 h (**Supplementary Fig. 32**). To quench the reaction, 800 μL of ethyl acetate and 40 μL of 2-hydroxyindole (100 mM stock) were added. The plate was then sealed with an organic-resistant mat

and shaken overnight at 900 rpm. After centrifugation at 3,000 g for 10 min, approximately 600 µL of the supernatant was collected, transferred to a new 96-deep well plate, and air-dried in a chemical hood. The resulting residues were then resuspended in 300 µL methanol. Following another centrifugation at 3,000 g for 10 min, 100 µL of the supernatant was collected and analyzed by LC-MS.

Fed-batch fermentation. For fed-batch fermentations in bench-top bioreactors (DASbox, Eppendorf, Hamburg, Germany), single colonies of *E. coli* BL21(DE3) strains were inoculated into 5 mL of LB medium supplemented with appropriate antibiotics and cultured overnight at 37 °C with shaking at 250 rpm. In the following day, 2 mL of seed culture was transferred into 200 mL of LB medium, or M9 minimal medium (Na_2HPO_4 30 g L^{-1}, KH_2PO_4, 15 g L^{-1}, NaCl 2.5 g L^{-1}, NH_4Cl 5 g L^{-1}, Thiamine-HCl 50 mg L^{-1}, Glucose 1 g L^{-1}, 1 M $MgSO_4$•$7H_2O$ 2 mL L^{-1}, Trace elements (92949-25ML, Sigma) 1 mL L^{-1}, Amino acid mixture (CSM, 114500012-CF, MP Biomedicals) 0.79 g L^{-1}, Tyrosine 2.5 mM, Tryptophan 2.5 mM), containing a low concentration of glucose (0.5-1 g L^{-1}) in the DASbox bioreactor. The cultures were incubated at 37 °C with an agitation speed of 250 rpm, while the pH was maintained at 6.5 using 4 N HCl and 10 M NaOH. To ensure sufficient oxygen availability, industrial-grade O_2 gas was continuously sparged into the bioreactors, maintaining a dissolved oxygen (DO) level of 30%. To control foaming, a drop of Antifoam 204 was added as needed. After approximately 5 hours of cultivation, when the OD600 reached 2.5-3.5, the temperature was lowered to 25 °C, and IPTG was added to a final concentration of 0.1 mM to induce protein expression. The fermentation continued under aerobic conditions to facilitate substrate accumulation. Once specific fermentation conditions were met, the process transitioned to an anaerobic phase by switching from O_2 to N_2 sparging. The N_2 supply was maintained for approximately 10 hours to deplete residual O_2, ensuring anaerobic conditions. Subsequently, 10 mM radical precursors were added for semi-photobiosynthetic fed-batch fermentation, or 1 mM FMN-Na was added for complete photobiosynthesis, prior to starting the illumination. To initiate photobiosynthesis, the cultures were illuminated with blue light using a Kessil PR160 Rig equipped with four 40 W, 440 nm blue LEDs (**Supplementary Fig. 33**). For fermentations utilizing pure glucose, an additional 50 g L^{-1} of glucose was supplemented into the bioreactors, while the pH was maintained at 6.5 using 4 N HCl and 10 M NaOH. Samples were collected at regular intervals to monitor product formation, glucose and substrate accumulation and consumption, and cell growth. Each fed-batch fermentation was conducted with two or three biological replicates to ensure reproducibility.

Cell viability assays. To evaluate the viability of *E. coli* BL21(DE3) during prolonged illumination under anaerobic conditions, live/dead staining was performed using the LIVE/DEAD® BacLight™ Bacterial Viability Kit (L7012, Thermo Fisher Scientific, USA). The procedures were modified based on the manufacturer's instructions. Cell samples were collected at defined time points and washed three times with PBS buffer. After the final wash, the cells were resuspended in PBS and diluted to an OD600 of approximately 0.2. For measurement, 100 µL of each cell suspension was transferred into individual wells of a 96-well flat-bottom microplate (in duplicate). To generate a standard curve, live and 70% isopropyl alcohol-killed cell suspensions were mixed in defined ratios (0:100, 10:90, 30:70, 50:50, 70:30, 90:10, and 100:0) and similarly distributed into wells. The staining solution was prepared by mixing 6 µL of Component A and 6 µL of Component B, followed by dilution with 2.0 mL of sterile deionized water to yield a 2X staining solution. Then, 100 µL of the 2X stain was added to each well, and the plate was mixed thoroughly by pipetting. After incubation in the dark at room temperature for 15 minutes, fluorescence was measured using a microplate reader with excitation at 485 nm, and emission collected at 530 nm (green, live cells) and 630 nm (red, dead cells). Cell viability was analyzed

by calculating the fluorescence intensity ratio (F_{530}/F_{630}) of each sample, with reference to the standard curve to determine the percentage of live cells.

$$(1)\ Ratio(\frac{G}{R}) = \frac{Fcell,em1}{Fcell,em2}$$

GC, GC/MS and HR-LC/MS analyses. Analysis of 4-vinylphenol, styrene, and indole was performed using an Agilent Technologies GC system equipped with a DB-5ms column (122-5532UI, Agilent). The GC oven temperature was initially maintained at 50 °C for 3 minutes, then ramped to 320 °C at a rate of 20 °C min^{-1}, and held at 320 °C for 1.5 minutes. For GC-MS analysis, an Agilent Technologies GC-MS system equipped with a DB-5ms column was used. The GC oven temperature was programmed to increase from 50 °C to 180 °C at a rate of 20 °C min^{-1}, followed by an increase to 315 °C at a rate of 50 °C min^{-1}. A solvent delay of 3 minutes was applied, and single ions of target products were detected.

For the enantioselectivity determination of the CPPB product, an Agilent Technologies GC system equipped with a Hydrodex g-TBDAc column (SN 23637-52, Macherey-Nagel) was used. The GC oven temperature was programmed to increase from 50 °C to 220 °C at a rate of 2.5 °C min^{-1}, followed by a 30-minute hold at 220 °C.

For HR-LC/MS detection, based on our previous study[49], samples were analyzed using a Q Exactive™ Orbitrap mass spectrometer (Thermo Fisher Scientific, USA) coupled with a Vanquish HPLC system (Thermo Fisher Scientific, USA). Chromatographic separation was performed on a Thermo Hypersil GOLD™ aQ column (3 µm, 2.1 × 150 mm; PN 25303-152130). The mobile phases consisted of solvent A (water with 0.1% formic acid) and solvent B (acetonitrile with 0.1% formic acid). A linear gradient elution was applied from 5% to 95% solvent B over 18 minutes, followed by an isocratic hold at 95% B for 5 minutes, at a constant flow rate of 0.2 mL min^{-1}. The autosampler and column compartment were maintained at 4 °C and 25 °C, respectively. Mass spectrometric data were acquired in positive electrospray ionization mode. Full MS scans were performed with the following settings: scan range m/z 50–750, resolution 70,000 FWHM, AGC target 3×10^6, and maximum injection time (IT) of 100 ms. For MS/MS (MS^2) acquisition, the instrument was operated at a resolution of 17,500 FWHM, with an AGC target of 1×10^5 and a maximum IT of 50 ms.

Antimicrobial assays. The antimicrobial activities of the characterized compounds were evaluated against two fungal and 16 bacterial strains, including nine pathogenic strains, using the broth microdilution method same as in our previous study[49]. The indicator strains included *Saccharomyces cerevisiae* BY4741, *Issatchenkia orientalis*, *Bacillus halodurans* C-125, *Bacillus subtilis* ATCC 6633, *Lactococcus lactis* CNRZ 481, *Micrococcus luteus* ATCC 4698, *Pseudomonas fluorescens* Pf-5, *Pseudomonas putida* mt-2, *Streptococcus mutans* ATCC 25175, and the following pathogenic bacterial strains: *Acinetobacter baumannii* ATCC 19606, *Bacillus anthracis* str. Sterne, *Bacillus cereus* TZ417, *Enterobacter cloacae*, vancomycin-resistant *Enterococcus faecium* U503 (VRE), *Klebsiella pneumoniae* ATCC 27736, *Pseudomonas aeruginosa* PA01, methicillin-resistant *Staphylococcus aureus* USA300 (MRSA), and *Staphylococcus epidermidis* 15×154. Fungi were inoculated from glycerol stocks and cultured in 5 mL YPD medium at 30 °C on a rotary shaker (250 rpm). *B. cereus*, *B. halodurans*, *B. subtilis*, and *M. luteus* were grown in 5 mL Tryptic Soy Broth (TSB) at 30 °C, while *E. cloacae*, *P. fluorescens*, and *P. putida* were cultured in Nutrient Broth (NB) at 30 °C. *L. lactis* was grown in M17 Broth with 0.5% lactose at 30 °C, and the remaining bacterial strains were cultured in Brain Heart Infusion (BHI) medium at 37 °C. Overnight cultures were diluted into fresh sterilized

medium and regrown to reach an OD600 of 0.04-0.06. The cells were then diluted 10-fold in fresh medium to achieve a final concentration of approximately 10^6 CFU/mL and distributed into 96-well microtiter plates. The wells were supplemented with test compounds at concentrations ranging from 64 to 0.0625 μg mL^{-1}. The Minimum Inhibitory Concentration (MIC) was determined as the lowest concentration at which no visible growth was observed after 16-18 hours of incubation. All experiments were performed in triplicate, with ampicillin (Amp) and hygromycin (Hyg) included as positive controls for antibacterial assays. For the antimicrobial activity assay against *E. coli*, *E. coli* BL21(DE3) cultures were adjusted to an initial OD600 of 0.5, and 1 mL aliquots were distributed into separate groups. The cell cultures were treated with a series of DIEP concentrations dissolved in DMSO (50, 100, 200, 300, 400, 500, 600, 700, 800, and 1000 mg L^{-1}), alongside control groups without compounds or with DMSO alone. After 24 h of treatment, the OD600 of each group was measured. Data were analyzed using GraphPad Prism 8.0.

Data availability

The DNA sequences of plasmids used in this study have been provided in the Supplementary Information. The other data are available in the main text, Supplementary Information, Source data, or from the authors upon reasonable request. The SnapGene files for the key plasmids can be accessed at: https://doi.org/10.5061/dryad.ns1rn8q54.

Acknowledgements

We thank Lucienne Burrus and Teresa Martin for their assistance with the fed batch fermentation experiments. This work was funded by the DOE Center for Advanced Bioenergy and Bioproducts Innovation, under the auspices of the US Department of Energy (DOE), Office of Science, Office of Biological and Environmental Research (award no. DE-SC0018420 to H.Z.). The funders had no role in the study design, data collection and analysis, decision to publish, or preparation of the manuscript.

Author contributions

The project was coordinated by H.Z., and H.Z., Y.Y. and M.L. jointly conceptualized the project and designed the research experiments. Y.Y., M.L. and H.Z. wrote the manuscript with input from all of the other authors. Y.Y. executed the strains construction, biosynthesis and fed batch fermentation experiments. Y.Y. and M.L. constructed the plasmids. M.L. synthesized the product standards. W.H. contributed to the construction of mutant library. W.H. and Z.Z. were responsible for synthesizing some radical precursors.

Competing interests

The authors declare no competing interests.

References

1 Yang, Y. & Arnold, F. H. Navigating the unnatural reaction space: Directed evolution of heme proteins for selective carbene and nitrene transfer. *Acc. Chem. Res.* **54**, 1209-1225 (2021).

2 Hanefeld, U., Hollmann, F. & Paul, C. E. Biocatalysis making waves in organic chemistry. *Chem. Soc. Rev.* **51**, 594-627 (2022).

3 Emmanuel, M. A. *et al.* Photobiocatalytic strategies for organic synthesis. *Chem. Rev.* **123**,

5459-5520 (2023).
4 Buller, R. *et al.* From nature to industry: Harnessing enzymes for biocatalysis. *Science* **382**, eadh8615 (2023).
5 Morita, I. & Ward, T. R. Recent advances in the design and optimization of artificial metalloenzymes. *Curr. Opin. Chem. Biol.* **81**, 102508 (2024).
6 Kissman, E. N. *et al.* Expanding chemistry through *in vitro* and *in vivo* biocatalysis. *Nature* **631**, 37-48 (2024).
7 Brouwer, B. *et al.* Noncanonical amino acids: Bringing new-to-nature functionalities to biocatalysis. *Chem. Rev.* **124**, 10877-10923 (2024).
8 Birch-Price, Z., Hardy, F. J., Lister, T. M., Kohn, A. R. & Green, A. P. Noncanonical amino acids in biocatalysis. *Chem. Rev.* **124**, 8740-8786 (2024).
9 Wu, S. *et al.* Biocatalysis: Enzymatic synthesis for industrial applications. *Angew. Chem. Int. Ed.* **60**, 88-119 (2021).
10 Peng, Y. *et al.* Recent advances in photobiocatalysis for selective organic synthesis. *Org. Process Res. Dev.* **26**, 1900-1913 (2022).
11 Yu, J. *et al.* Single-electron oxidation triggered by visible-light-excited enzymes for asymmetric biocatalysis. *Angew. Chem. Int. Ed.* **64**, e202419262 (2025).
12 Harrison, W. *et al.* Photobiocatalysis for abiological transformations. *Acc. Chem. Res.* **55**, 1087-1096 (2022).
13 Fu, H. & Hyster, T. K. From ground-state to excited-state activation modes: Flavin-dependent "ene"-reductases catalyzed non-natural radical reactions. *Acc. Chem. Res.***57**, 1446-1457 (2024).
14 Jain, S., Ospina, F. & Hammer, S. C. A new age of biocatalysis enabled by generic activation modes. *JACS Au* **4**, 2068-2080 (2024).
15 Cheng, L. *et al.* Stereoselective amino acid synthesis by synergistic photoredox-pyridoxal radical biocatalysis. *Science* **381**, 444-451 (2023).
16 Wang, T.-C. *et al.* Stereoselective amino acid synthesis by photobiocatalytic oxidative coupling. *Nature* **629**, 98-104 (2024).
17 Xu, Y. *et al.* A light-driven enzymatic enantioselective radical acylation. *Nature* **625**, 74-78 (2024).
18 Xing, Z. *et al.* Synergistic photobiocatalysis for enantioselective triple-radical sorting. *Nature* **637**, 1118-1123 (2025).
19 Sun, N. *et al.* Enantioselective [2+2]-cycloadditions with triplet photoenzymes. *Nature* **611**, 715-720 (2022).
20 Trimble, J. S. *et al.* A designed photoenzyme for enantioselective [2+2] cycloadditions. *Nature* **611**, 709-714 (2022).
21 Guo, J. *et al.* Chemogenetic evolution of diversified photoenzymes for enantioselective [2 + 2] cycloadditions in whole cells. *J. Am. Chem. Soc.* **146**, 19030-19041 (2024).
22 Tseliou, V. *et al.* Stereospecific radical coupling with a non-natural photodecarboxylase. *Nature* **634**, 848-854 (2024).
23 Fu, Y. *et al.* Whole-cell-catalyzed hydrogenation/deuteration of aryl halides with a genetically repurposed photodehalogenase. *Chem* **9**, 1897-1909 (2023).
24 Hirschi, S. *et al.* Synthetic biology: Bottom-up assembly of molecular systems. *Chem. Rev.* **122**, 16294-16328 (2022).
25 Ro, D.-K. *et al.* Production of the antimalarial drug precursor artemisinic acid in engineered

yeast. *Nature* **440**, 940-943 (2006).
26 Luo, X. *et al.* Complete biosynthesis of cannabinoids and their unnatural analogues in yeast. *Nature* **567**, 123-126 (2019).
27 Zhang, J. *et al.* A microbial supply chain for production of the anti-cancer drug vinblastine. *Nature* **609**, 341-347 (2022).
28 Gao, J. *et al.* Biosynthesis of catharanthine in engineered *Pichia pastoris*. *Nat. Synth.* **2**, 231-242 (2023).
29 Liu, Y. *et al.* Complete biosynthesis of qs-21 in engineered yeast. *Nature*, 1-8 (2024).
30 Huang, J. *et al.* Unnatural biosynthesis by an engineered microorganism with heterologously expressed natural enzymes and an artificial metalloenzyme. *Nat. Chem.* **13**, 1186-1191 (2021).
31 Huang, J. *et al.* Complete integration of carbene-transfer chemistry into biosynthesis. *Nature* **617**, 403-408 (2023).
32 Li, M. *et al.* Asymmetric photoenzymatic incorporation of fluorinated motifs into olefins. *Science* **385**, 416-421 (2024).
33 Duan, X. *et al.* Ground-state flavin-dependent enzymes catalyzed enantioselective radical trifluoromethylation. *Nat. Commun.* **16**, 1225 (2025).
34 Qi, W. W. *et al.* Functional expression of prokaryotic and eukaryotic genes in *Escherichia coli* for conversion of glucose to p-hydroxystyrene. *Metab. Eng.* **9**, 268-276 (2007).
35 Lee, W.-H., Kim, M.-D., Jin, Y.-S. & Seo, J.-H. Engineering of NADPH regenerators in *Escherichia coli* for enhanced biotransformation. *Appl. Microbiol. Biotechnol.* **97**, 2761-2772 (2013).
36 Ajikumar, P. K. *et al.* Isoprenoid pathway optimization for taxol precursor overproduction in *Escherichia coli*. *Science* **330**, 70-74 (2010).
37 McKenna, R. & Nielsen, D. R. Styrene biosynthesis from glucose by engineered *Escherichia coli*. *Metab. Eng.* **13**, 544-554 (2011).
38 Huang, X. *et al.* Photoenzymatic enantioselective intermolecular radical hydroalkylation. *Nature* **584**, 69-74 (2020).
39 Li, M. *et al.* Remote stereocontrol with azaarenes via enzymatic hydrogen atom transfer. *Nat. Chem.* **16**, 277-284 (2024).
40 Liu, Y. *et al.* Asymmetric synthesis of alpha-chloroamides via photoenzymatic hydroalkylation of olefins. *J. Am. Chem. Soc.* **146**, 7191-7197 (2024).
41 Chen, X. *et al.* Photoenzymatic hydrosulfonylation for the stereoselective synthesis of chiral sulfones. *Angew. Chem. Int. Ed.* **62**, e202218140 (2023).
42 Harrison, W. *et al.* Photoenzymatic asymmetric hydroamination for chiral alkyl amine synthesis. *J. Am. Chem. Soc.* **146**, 10716-10722 (2024).
43 Kumari, A. & Singh, R. K. Medicinal chemistry of indole derivatives: Current to future therapeutic prospectives. *Bioorg. Chem.* **89**, 103021 (2019).
44 Zhao, B. *et al.* Direct visible-light-excited flavoproteins for redox-neutral asymmetric radical hydroarylation. *Nat. Catal.* **6**, 996-1004 (2023).
45 Lee, J.-H. & Lee, J. Indole as an intercellular signal in microbial communities. *FEMS Microbiol. Rev.* **34**, 426-444 (2010).
46 Das, A. *et al. Methods in enzymology*. Vol. 693, 1-30 (Elsevier, 2023).
47 Shimizu, K. & Matsuoka, Y. Feedback regulation and coordination of the main metabolism for bacterial growth and metabolic engineering for amino acid fermentation. *Biotechnol. Adv.* **55**,

107887 (2022).
48 Trott, O. & Olson, A. J. Autodock vina: Improving the speed and accuracy of docking with a new scoring function, efficient optimization, and multithreading. *J. Comput. Chem.* **31**, 455-461 (2010).
49 Yuan, Y. *et al.* Self-resistance-gene-guided, high-throughput automated genome mining of bioactive natural products from *streptomyces*. *Cell Syst.* **16**, 101237 (2025).